

Magnetotelluric monitoring of hydraulic fracture stimulation at the Habanero Enhanced Geothermal System, Cooper Basin, South Australia

Yohannes L. Didana*
University of Adelaide
Adelaide, Australia
yohannes.didana@adelaide.edu.au

Stephan Thiel
GSSA
Adelaide, Australia

Graham Heinson
University of Adelaide
Adelaide, Australia

Goren Boran
University of Adelaide
Adelaide, Australia

SUMMARY

Magnetotelluric (MT) data were collected across the Habanero Enhanced Geothermal System project in the Cooper Basin, South Australia. A baseline regional MT survey consisting of two profiles was collected to delineate the pre-injection resistivity structure. Two dimensional inversions of the MT data reveal three main resistivity structures to a depth of 5 km. The low resistivity surface layer (about 1.5 km thick) is interpreted as poorly consolidated sediments of Lake Eyre and Eromanga Basins. Below the conductive layer, a zone with relatively high resistivity with thickness of 2 km can be correlated to consolidated Cooper Basin sediments. A high resistivity zone below depths of 3.5 km is interpreted as the hot intrusive granodiorite (granite) of the Big Lake Suite with low porosity and permeability. This deep structure is also related to the Habanero EGS reservoir.

The second MT survey was conducted during stimulation of Habanero-4 well by Geodynamics Ltd, where 36.5 ML of water with a resistivity of 13 Ωm (at 25°C) was injected at a relatively continuous rate of between 27-53 L/s over 14 days at a depth of almost 4 km. Analysis of pre- and post-injection residual phase tensors for periods greater than 10 s indicate conductive fractures oriented in a N/NNE direction. Apparent resistivity maps also revealed that injected fluids possibly propagated towards N/NNE direction. This result is in agreement with the micro-seismic events with an area of 4 km² observed during fluid injection, as well as orientation of pre-existing N-S striking sub-horizontal fractures susceptible to slip due to stimulation. The MT responses close to injection show on average 5% decrease in apparent resistivity at periods greater than 10 s. The main reasons for observing subtle changes in resistivity at Habanero EGS is the screening effect of the conductive thick sedimentary cover (about 3.6 km thick) and the presence of pre-existing saline fluids with resistivity of 0.1 Ωm (equivalent to salinity of 16.1 g/L at 240°C) in the natural fractures. Overall, the MT monitoring at Habanero EGS highlights the need for favourable geological settings to measure significant changes in resistivity in EGS reservoirs.

Key words: Magnetotelluric Monitoring, fluid injection, Enhanced geothermal system (EGS), Habanero.

INTRODUCTION

Enhanced geothermal systems (EGS) are unconventional geothermal resources with low permeability and relatively high temperature (typically > 200°C), which require fluid stimulation to enhance hydraulic connectivity in existing fracture system (Audigane, et al. 2002, Evans, et al. 2005, Muñoz 2014). A significant number of EGS potential resources occur around the world in varying geological settings e.g. (Bendall, et al. 2014, Chamorro, et al. 2014, DiPippo 2012, Ziagos, et al. 2013). The productivity of EGS reservoirs critically depends on the permeability of the fractures in the host rock.

Micro-seismics is the main geophysical method used to investigate fractures opened during hydraulic stimulation (Baisch, et al. 2015, Baria, et al. 2004, Cladouhos, et al. 2013, Cuenot, et al. 2008). It gives information about opening of fractures; however, it does not provide information about fluid movement or fracture inter-connectivity (Cladouhos, et al. 2013). On the other hand, magnetotellurics (MT) has been used to image electrically conductive fluid-filled fractures in EGS reservoirs to a depth of 4-5 km (MacFarlane, et al. 2014, Peacock, et al. 2013, Peacock, et al. 2012).

Bedrosian et al. (2004) conducted the first MT monitoring studies around a natural gas exploration well in the North German Basin during hydraulic stimulation at a depth of 4 km. The 2D MT models did not recover changes in subsurface resistivity following the fluid injection because of low data quality (low signal-to-noise ratio) (Bedrosian, et al. 2004). Peacock et al., (2012) and Peacock et al. (2013) also used MT for monitoring the injection of 3.1 ML of saline fluids into an EGS reservoir at a depth of 3.6 km at Paralana, South Australia, over a period of 4 days. The MT responses from the pre- and post-injection data showed an average decrease of 10% and 5% in the xy and yx components of apparent resistivity, respectively (Peacock, et al. 2013, Peacock, et al. 2012). Furthermore, using residual phase tensor analysis, (Peacock, et al. 2013) demonstrated that the injected fluids propagated along pre-existing fault system oriented in a NNE direction. The micro-seismic survey conducted at Paralana EGS showed fractures opened in a NNE, NE, and ENE direction along pre-existing fault systems (Albaric, et al. 2014, Hasting, et al. 2011). These studies showed the complementarity of MT and micro-seismics in characterizing fluid injection into EGS reservoirs.

The Habanero EGS project is Australia's most advanced deep geothermal project and is located in South Australia about 800 km NE of Adelaide (Figure 1). The area is characterized by relatively high surface heat flow, with an average heat flow of 100 mW/m²

ascribed to high heat producing granites (Beardsmore 2004, Meixner, et al. 2012). Four EGS wells have been drilled into the hot granitic basement to a maximum depth of 4.3 km with a maximum downhole temperature of 244°C (Hogarth, et al. 2013). The Cooper and Eromanga sedimentary basins (~3.6 km thick) act as an insulating cap over the granitic EGS reservoir (Holl and Barton 2015). The project area is characterized by a compressive stress field oriented approximately in E-W direction (Reynolds, et al. 2006, Reynolds, et al. 2005).

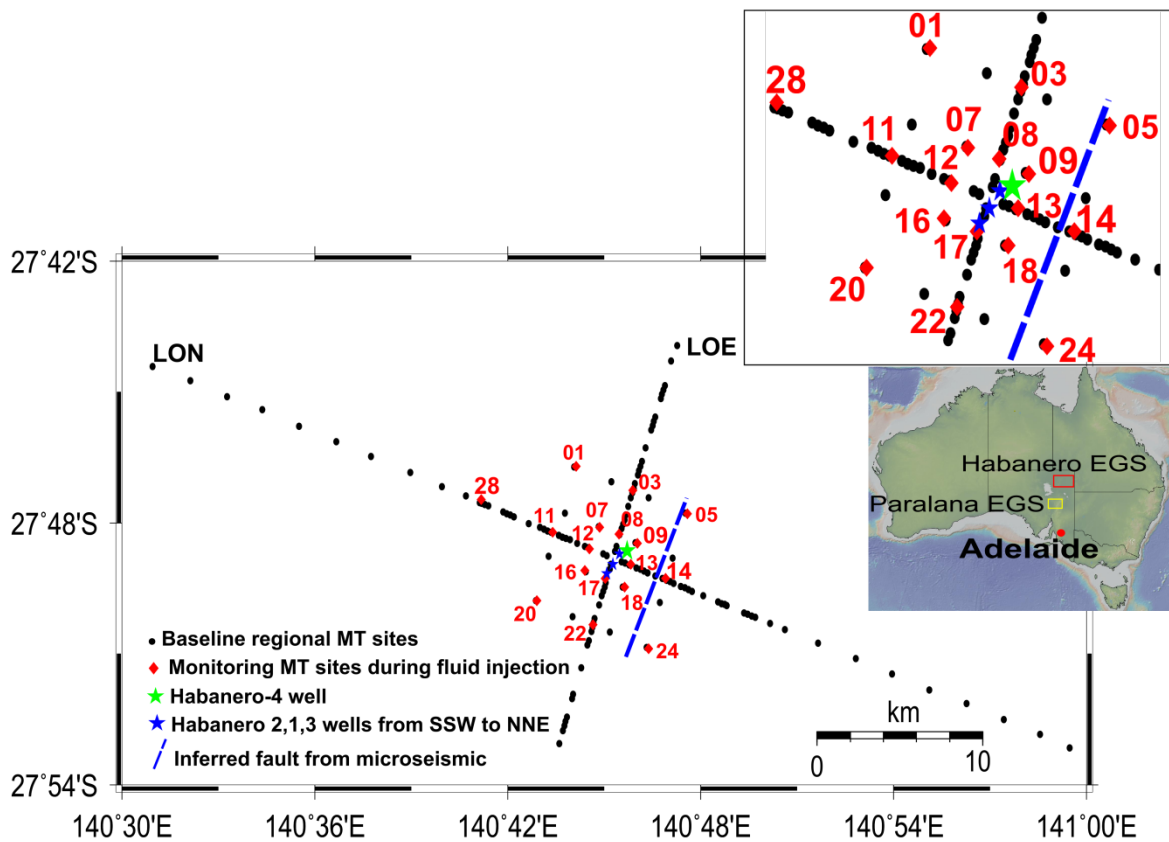


Figure 1: Location map of MT sites at the Habanero EGS located in South Australia. Black dots denote MT stations from Quantec Geoscience Ltd recorded before stimulation (baseline survey) in August, 2012. The red diamonds denote broadband MT stations acquired by University of Adelaide during fluid injection of the Habanero-4 well, which lasted for 19 days (November 15– December 3, 2012). Green star Habanero-4 well and blue stars are Habanero-2, 1, 3 wells from SSW to NNE, respectively. The red square on the inset map of Australia is the Habanero EGS project area. The yellow square on the inset map of Australia is the Paralana EGS project area. The central part of the location map is enlarged in size on the inset for visualization.

In November 2012, the Habanero-4 well was stimulated by injecting 36.5 ML of near-surface aquifer-sourced water (13 Ω m at 25°C) over 14 days (Hogarth, et al. 2013, Holl and Barton 2015, McMahon and Baisch 2013). During the extended stimulation, 20200 micro-seismic events were located (McMahon and Baisch 2013). The main target of the stimulation was a sub-horizontal fracture zone (~5 - 10 m thick and dipping 10° to the west south west) at a depth of 4077 m in the hot granitic reservoir (Baisch, et al. 2015, Bendall, et al. 2014, McMahon and Baisch 2015). This sub-horizontal fracture zone (Habanero fault) is crossed by all Habanero EGS wells (Bendall, et al. 2014, McMahon and Baisch 2013) and is the permeable reservoir of the Habanero EGS system.

The goal of this project is to use MT to monitor temporal and spatial changes in subsurface bulk resistivity structure caused by enhanced permeability due to injected fluids. We first collected a baseline survey along two profile lines before the fluid injection and created 2D resistivity models. Then we set out stations just before the injection and continuously collected data till 3 days after the hydraulic stimulation for a total of 19 days. We analysed the monitoring data using resistivity maps and residual phase tensor.

METHOD

Magnetotellurics is a passive electromagnetic geophysical method used to investigate the distribution of electrical resistivity of the Earth (Chave and Jones 2012). In the MT method, orthogonal components of natural horizontal electric (\mathbf{E}) and magnetic (\mathbf{H}) fields are measured simultaneously as a function of time and converted to frequency domain using Fourier transformation in order to determine the resistivity structure under the survey area. The horizontal electric and magnetic fields are related by the impedance

tensor (\mathbf{Z}) given by $\mathbf{E}=\mathbf{ZH}$. Apparent resistivity ρ_a as a function of frequency f is given by $\rho_a = \frac{1}{\mu\omega} \left| \frac{E_i}{H_j} \right|^2$, with $\omega = 2\pi f$

where μ is magnetic permeability and ω is angular frequency of the source signal. The electromagnetic skin depth (depth of investigation) is approximately $P(T) \approx 0.5\sqrt{T\rho_a} \text{ km}$ where ρ_a is apparent resistivity, or the average resistivity of an equivalent half space and T is the period in seconds. The complex impedance tensor can be written in terms of its real (\mathbf{X}) and imaginary (\mathbf{Y}) parts as $\mathbf{Z} = \mathbf{X} + i\mathbf{Y}$. Another way of representing the MT response is by the MT phase tensor, which is defined by the relation $\Phi = \mathbf{X}^{-1}\mathbf{Y}$ and is not affected by galvanic distortion (Booker 2014, Caldwell, et al. 2004).

The bulk electrical conductivity (σ_{bulk}) of a consolidated formation with undamaged interconnected pore spaces during rock deformation can be estimated from the electrical conductivity of a fluid (σ_f) and the hydrologic permeability (k) by using $\sigma_{bulk} = \sigma_f(k/\alpha)^{2/3}$ with $\alpha = 1 \times 10^{-12} \text{ m}^2$ (Spichak and Manzella 2009, Zhang, et al. 1994). However, these petrological properties are not always directly related as conductivity and permeability of a formation increase or decrease differently with temperature, pressure and depth (Spichak and Manzella 2009).

Phase tensor residuals give information about geo-electric strike transformation during fluid injection and help to identify the direction of maximum change in current flow (Booker 2014, Heise, et al. 2007, Peacock, et al. 2013). The residual phase tensor is calculated as $\Delta\Phi_{12} = I - (\Phi_2^{-1}\Phi_1)$, where $\Phi_2, \Phi_1, I, \Phi^{-1}$ are the phase tensor post-injection, the phase tensor pre-injection, the identity matrix of rank two and the inverse of phase tensor, respectively.

A total of 135 MT soundings were acquired by Quantec Geoscience Ltd at the Habanero EGS project of Geodynamics in August 2012 as a baseline measurement (Figure 1). The MT sites were set up in two perpendicular profiles with infill sites in a square grid at the center of the Habanero EGS field (Figure 1). The MT soundings cover broadband frequencies in the range of 0.004 to 1000 s. Remote reference sites were established at a distance of 20 km to the NE of the survey area. The electric dipole length used was 200 m. A typical resistivity and phase curve from the baseline regional survey, which has too small error bars, is shown on Figure 2. The resistivity and phase curve show the 1D nature of the sounding. Static shifts observed on few sites were corrected by moving a curve up or down by comparing it with neighboring sites and sticking the resistivity curves together at high frequencies using WinGLink software (Rodi and Mackie 2001).

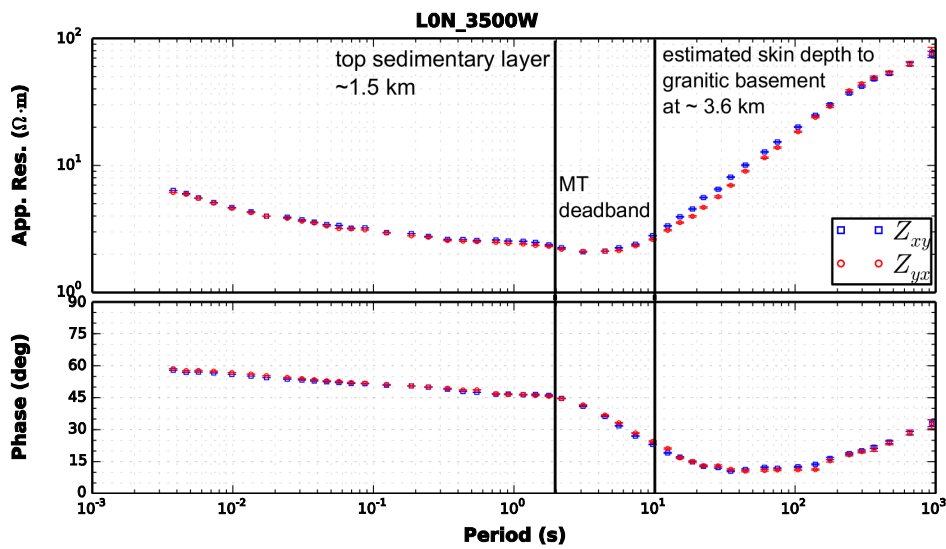


Figure 2: Example of resistivity phase curve from the baseline survey. The blue squares and the red circles denote xy and yx components of resistivity and phases, respectively. The resistivity and phase curve show the 1D nature of the sounding.

The second time-lapse MT survey was conducted during fluid injection of well Habanero-4 by Geodynamics Ltd, over 14 days. The MT data recording was started two day before the fluid injection. The data were acquired from a total of 17 MT sites in a rectangular grid by the University of Adelaide using the AUSCOPE MT broadband instrument (Figure 1). At each site, data were continuously recorded at a sampling rate of 500 Hz covering a period range from 0.01 to 1000 s including pre-injection, during injection and post-injection for 19 days (15 November - 3 December, 2012). The sites were briefly stopped for electrode replenishment every three days. The electric dipole length used was 50 m. The time series were processed using the robust processing BRIPP5 code (Chave and Thomson 2004) resulting in good impedance estimates for periods of 0.01 s to 100 s except low quality data at the dead band for some sites. The processed MT data have a good repeatability across the successive days and small measurement error in resistivity (about 1-2%) and phase (about 1-3%). However, few days of recordings of site 13, which is 650 m away from the Habanero-4 well, was affected by noise from the fluid injection operation. For this reason, the segments of the time series, in which the activity of the operation was minimal, were selected for processing of site 13 MT data set. Static shifts observed at a site on successive days were corrected by moving a resistivity curve up or down (by comparing it with neighboring sites) and sticking the resistivity curves together at high frequencies and making sure that all the resistivity curves have same resistivity at the highest frequency using WinGLink program (Rodi and Mackie 2001). A typical sounding curve from the time-lapse monitoring survey is shown in Figure 3.

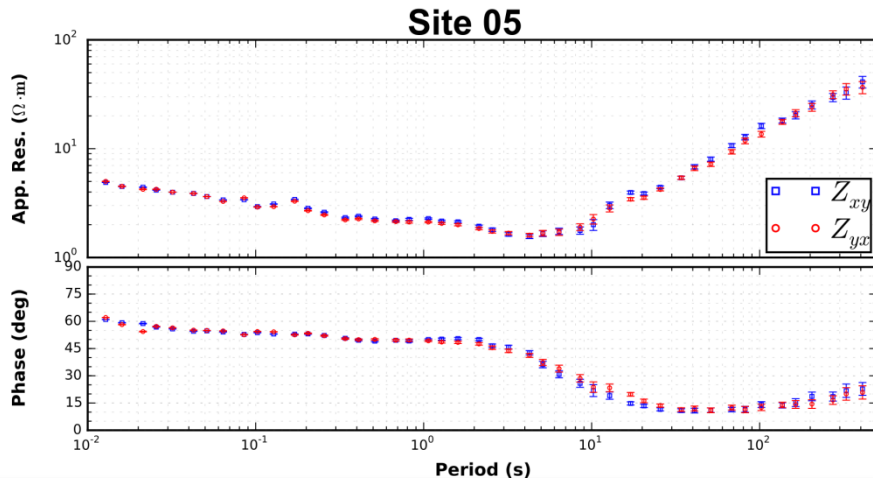


Figure 3: Example of resistivity phase curve for site 05 from the time-lapse MT monitoring survey. The blue squares and the red circles denote xy and yx components of resistivity and phases, respectively.

RESULTS

The MT data were inverted using the MARE2DEM 2D inversion code, which is a goal-oriented adaptive finite element code for MT that allows an unstructured model grid (Key and Ovall 2011). A total of 53 periods (0.004 s – 655 s) were used for the inversion. Error floors of 10% and 5% were used for resistivities and phases for the inversion, respectively. Different 2D inversions of the MT data with different starting models were carried out. These include homogeneous half space of 10 Ωm, 100 Ωm and a three layered Earth model based on resistivity logs (with resistivities and thicknesses of 3 Ωm/1600 m, 20 Ωm/1000 m, 100 Ωm half space). All the inversions resulted in similar models. At a depth of 3 - 4.5 km in the central part of the profile, a fine mesh grid was used in order to resolve possible structures in the EGS reservoir. The preferred model using a starting model of homogeneous half space of 100 Ωm from the joint inversion of TE and TM mode for profile LON is presented in Figure 4 (location of the profile is shown in Figure 1). The models reveal three main resistivity structures to a depth of 5 km. The low resistivity structure surface layer (C), which is about 1.5 km thick, is associated with areas of poorly consolidated sands, siltstones and clay stones of Lake Eyre and Eromanga Basin. The intermediate resistivity structure (R1) can be correlated to consolidated sandstones, siltstones and shales of the Cooper basin (natural gas and petroleum reservoir rocks). The high resistivity structure at depth of about 3.5 km (R2) is interpreted as the intrusive granodiorite (granite) of the Big Lake Suite with low porosity and permeability (Holl and Barton 2015, McMahon and Baisch 2015, Meixner, et al. 2000).

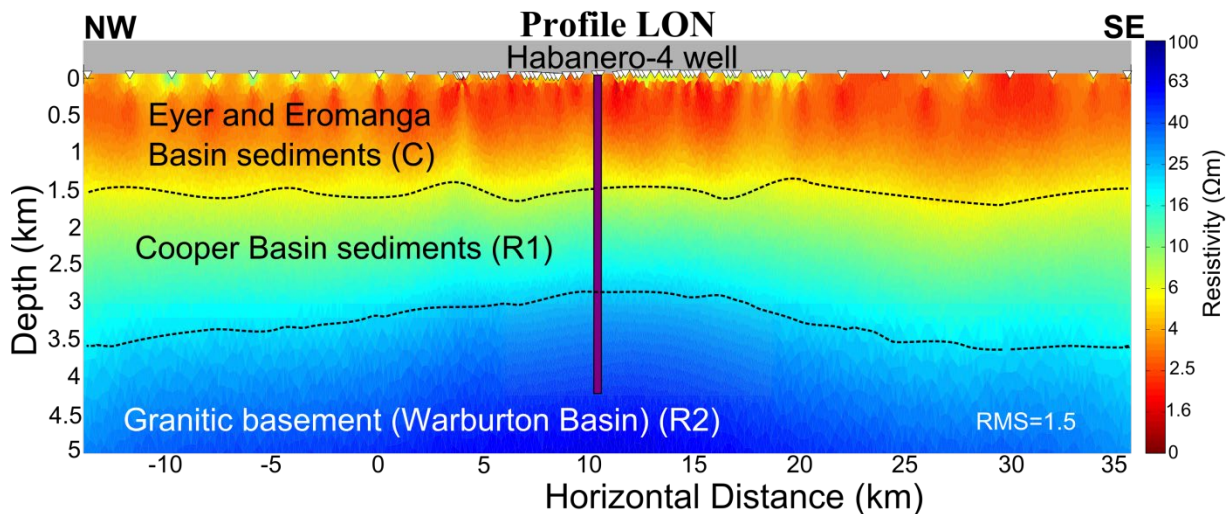


Figure 4: Preferred 2D resistivity model obtained by joint inversion of TE and TM modes data for profile LON with a RMS misfit of 1.5. C is a low resistivity layer. R1 is intermediate resistivity layer and R2 is a high resistivity layer.

A decrease in resistivity due to simulation of Habanero-4 well at 4 km depth is expected to occur at a period greater than 10 s. A typical resistivity phase curve for pre- and post-injection for site 09 which is located 870 m NE of Habanero-4 is shown in Figure 5 (refer to Figure 1 for location of site 09). The xy component of the resistivity curve shows on average a 5% decrease in resistivity values at periods greater than 10 s post-injection (Figure 5a). However, the yx component of resistivity curve indicates on average a 1.5% decrease in resistivity in these periods post-injection (Figure 5b). This demonstrates the directional nature of the maximum current flow in the fractures.

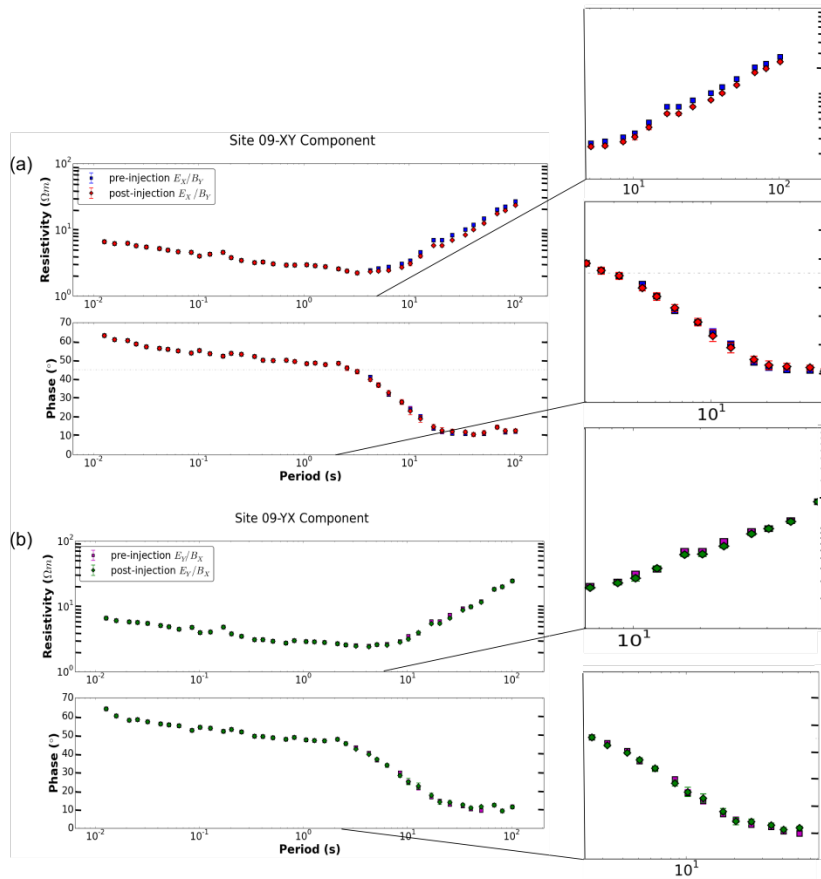


Figure 5: Resistivity phase curves pre- and post-injection for site 09. (a) xy component resistivity phase curve (b) yx component resistivity phase curve. The average decrease in resistivity for site 09 is about 5% in the xy component and 1.5% in the yx component at periods greater than 10 s post-injection. The blue and magenta squares are pre-injection curves. The red and green diamonds are post-injection curves.

Apparent resistivity maps of the xy component at selected periods of 0.05 s, 17 s, and 34 s for days 1, 5, 10 and 19 of time-lapse monitoring is shown in Figure 6. At a period of 0.05 s, all the resistivity maps of the respective days show similar resistivity structure (Figure 6a-d). Regions marked as “B” with apparent resistivities of < 3.3 Ω m at period of 17 s and < 6 Ωm at period of 34 s in the NE sector on the resistivity maps show a decrease in resistivity for day 5, day 10 and day 19 (Figure 6f-h, k-m) compared to day 1 (Figure 6e,i) of the fluid injection monitoring surveys. However, regions marked as “A” with apparent resistivities > 3.8 Ωm at period of 17 s and > 7 Ωm at period of 34 s, which are located in the NW and SE sector, do not reveal change in resistivity for day 5, day 10 and day 19 (Figure 6f-h,k-m) compared to day 1 (Figure 6e,i) of the monitoring surveys. The apparent resistivity maps show possible direction of propagation of the injected fluid towards N/NNE despite the change in resistivity is marginal.

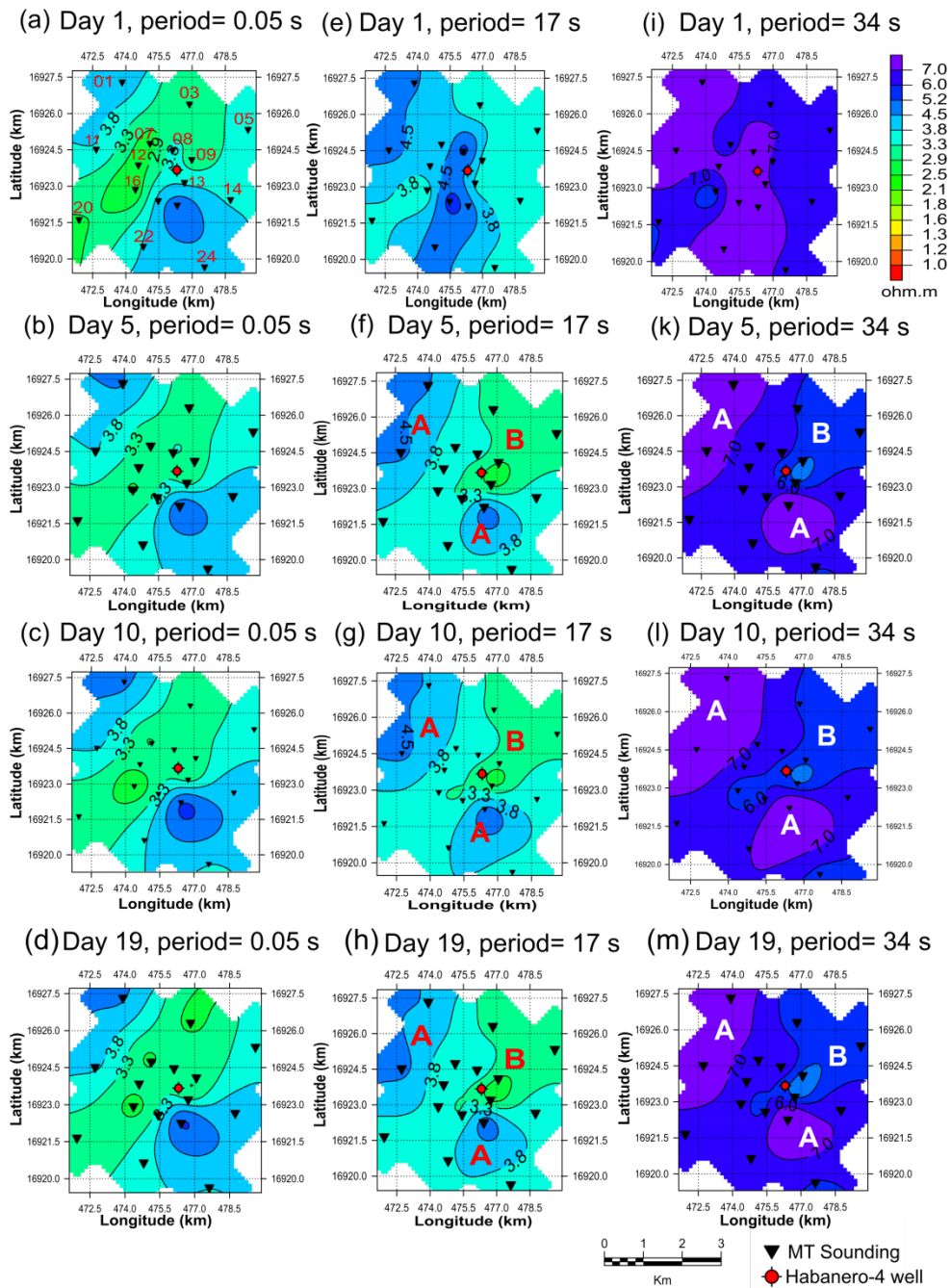


Figure 6: Apparent resistivity maps of the xy component for days 1, 5, 10 and 19 of time-lapse monitoring at selected periods of (a-d) 0.05s, (e-h) 17s, and (i-m) 34s. Regions marked as B show change in resistivity for day 5, day 10 and day 19 compared to day 1. However, regions marked as A do not reveal change in resistivity for day 5, day 10 and day 19 compared to day 1. The inverted triangles are MT sites of time-lapse monitoring. The red circle is Habanero-4 well.

The calculated residual phase tensor maps reveal changes due to stimulation at periods of about 10 s and later. The residual phase tensor plots reveal the direction of maximum current flow with the major axis of the ellipses aligned in N/NNE direction for most sites (Figure 7). This result is consistent with the propagation direction of micro-seismic events during hydraulic stimulation of Habanero-4 (Bendall, et al. 2014, Holl and Barton 2015, McMahon and Baisch 2015).

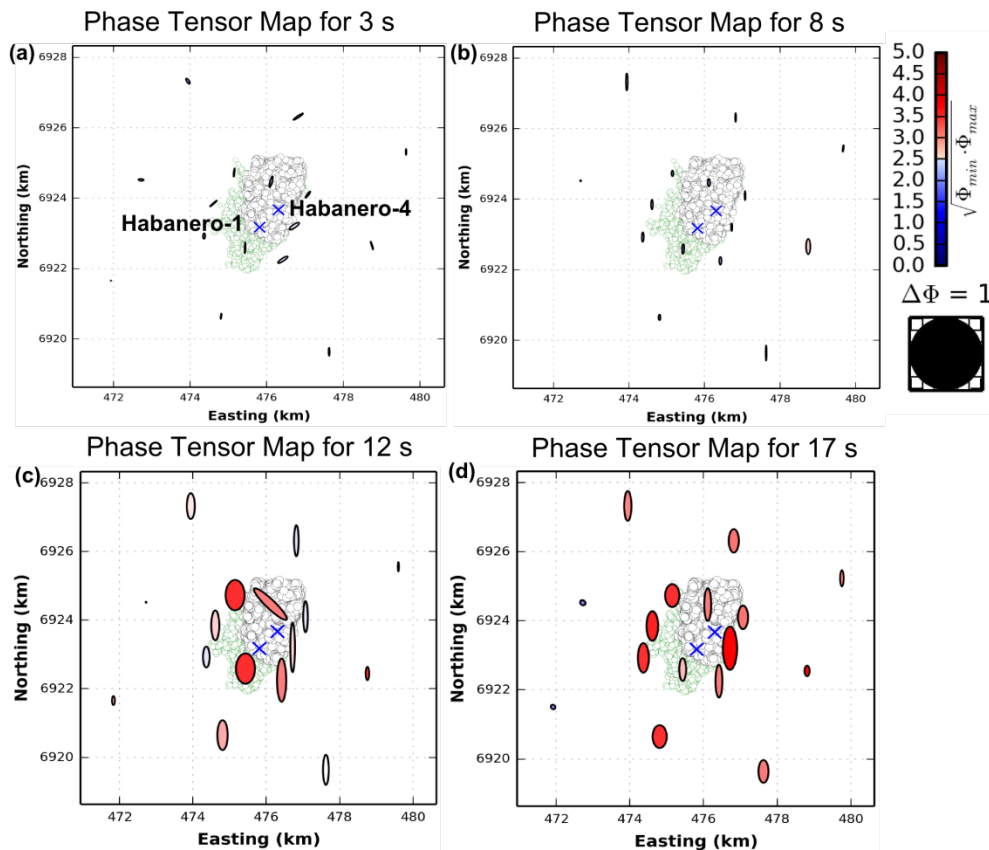


Figure 7: Maps of phase tensor residuals between pre- and post-stimulation measurements at period of (a) 3 s (b) 8 s (c) 12 s (d) 17 s. The green and black dots at the background represent the seismic cloud from micro-seismic data collected during stimulation of Habanero-1 and Habanero-4, respectively. The seismic clouds of the two stimulations overlap, with the 10 % increment in north direction in 2012 (McMahon and Baisch 2015). The blue “x” symbols are Habanero-1 (injection well towards south) and Habanero-4 (producer) wells. The ellipses are colored by percentage of the geometric mean of change in maximum and minimum phases. The ellipses are normalized by the maximum value of Φ_{max} .

CONCLUSIONS

Residual phase tensor analysis of MT measurements during a fluid injection show possible fluid-filled fractures oriented in a N/NE direction. Apparent resistivity maps also reveal the injected fluids probably propagated towards N/NE direction. This is consistent with the propagation direction of seismic events observed during fluid injection and the orientation of pre-existing horizontal fractures susceptible to slip in the over-thrust stress regime at the Habanero reservoir depth (Bendall, et al. 2014, Holl and Barton 2015, McMahon and Baisch 2013, McMahon and Baisch 2015). The observed decrease in resistivity at Habanero is small compared to the 10% average decrease in resistivity at Paralana during hydraulic stimulation (Peacock, et al. 2013). The main reasons for observing small changes in resistivity at Habanero EGS are the screening effect of the conductive sedimentary basin in the area (about 3.6 km thick) and the presence of pre-existing saline fluids with resistivity of $0.1 \Omega\text{m}$ (salinity of 16.1 g/L at 240°C) in the natural fractures in the EGS reservoirs (Hogarth, et al. 2013, Holl and Barton 2015, Meixner, et al. 2014, Yanagisawa, et al. 2011). Furthermore, the stimulated reservoir at Habanero is a granitic basement with low permeability while the targeted reservoir at Paralana is a neo-Proterozoic meta-sedimentary formation (Holl and Barton 2015, Llanos, et al. 2015, Meixner, et al. 2000, Peacock, et al. 2013). The time-lapse continuous monitoring MT study at Habanero highlights the need for favourable geological settings to achieve significant change in resistivity in EGS reservoirs. Despite these limitations, the MT method shows potential as a complementary method to micro-seismic in fluid monitoring for unconventional resource exploration because of its sensitivity to conductivity contrasts caused by fluids (Baria, et al. 2004, Börner, et al. 2015, Cladouhos, et al. 2013, Cuenot, et al. 2008, Peacock, et al. 2013, Peacock, et al. 2012, Wohlenberg and Keppeler 1987).

ACKNOWLEDGMENTS

The authors would like to thank the Australian Geophysical Observatory System (AGOS) for funding this research project. Yohannes L. Didana receives University of Adelaide ASI scholarship. Stephan Thiel is funded through the South Australian Centre for Geothermal Energy Research (SACGER). The authors also thank Geodynamics Ltd. for providing access to the geothermal project area to collect MT data and technical reports on Habanero EGS project. The authors are grateful to Heinz-Gerd Holl and Andrew McMahon from Geodynamics Ltd. for valuable discussions.

REFERENCES

- Albaric, J., Oye, V., Langet, N., Hasting, M., Lecomte, I., Iranpour, K., Messeiller, M., and Reid, P., 2014, Monitoring of Induced Seismicity During the First Geothermal Reservoir Stimulation at Paralana, Australia. *Geothermics* **52**, 120-31.
- Audigane, P., Royer, J.-J., and Kaieda, H., 2002, Permeability Characterization of the Soultz and Ogachi Large-Scale Reservoir Using Induced Microseismicity. *Geophysics* **67**, 204-11.
- Baisch, S., Rothert, E., Stang, H., Vörös, R., Koch, C., and McMahon, A., 2015, Continued Geothermal Reservoir Stimulation Experiments in the Cooper Basin (Australia). *Bulletin of the Seismological Society of America* **105**, 198-209.
- Baria, R., Michelet, S., Baumgärtner, J., Dyer, B., Gerard, A., Nicholls, J., Hettkamp, T., Teza, D., Soma, N., and Asanuma, H., Microseismic Monitoring of the World's Largest Potential Hdr Reservoir. *Twenty-Ninth Workshop on Geothermal Reservoir Engineering, Stanford University, Stanford, CA*.
- Beardsmore, G., 2004, The Influence of Basement on Surface Heat Flow in the Cooper Basin. *Exploration Geophysics* **35**, 223-35.
- Bedrosian, P., Weckmann, U., Ritter, O., Hammer, C., Hübert, J., and Jung, A., 2004, Electromagnetic Monitoring of the Groß Schönebeck Stimulation Experiment. *proceedings Jahrestagung der Deutschen Geophysikalischen Gessellschaft* **64**.
- Bendall, B., Hogarth, R., Holl, H., McMahon, A., Larking, A., and Reid, P., 2014. Australian Experiences in Egs Permeability Enhancement—a Review of 3 Case Studies. *Thirty-Ninth Workshop on Geothermal Reservoir Engineering*, 10.
- Booker, J.R., 2014, The Magnetotelluric Phase Tensor: A Critical Review. *Surveys in Geophysics* **35**, 7-40.
- Börner, J.H., Bär, M., and Spitzer, K., 2015, Electromagnetic Methods for Exploration and Monitoring of Enhanced Geothermal Systems – a Virtual Experiment. *Geothermics* **55**, 78-87.
- Caldwell, T.G., Bibby, H.M., and Brown, C., 2004, The Magnetotelluric Phase Tensor. *Geophysical Journal International* **158**, 457-69.
- Chamorro, C.R., García-Cuesta, J.L., Mondéjar, M.E., and Pérez-Madrado, A., 2014, Enhanced Geothermal Systems in Europe: An Estimation and Comparison of the Technical and Sustainable Potentials. *Energy* **65**, 250-63.
- Chave, A.D. and Jones, A.G., 2012, *The Magnetotelluric Method Theory and Practice*. Cambridge University Press.
- Chave, A.D. and Thomson, D.J., 2004, Bounded Influence Magnetotelluric Response Function Estimation. *Geophysical Journal International* **157**, 988-1006.
- Cladouhos, T.T., Petty, S., Nordin, Y., Moore, M., Grasso, K., Uddenberg, M., Swyer, M., Julian, B., and Foulger, G., 2013, Microseismic Monitoring of Newberry Volcano Egs Demonstration. *Proceedings of the 38th Workshop on Geothermal Reservoir Engineering, Stanford, CA*, 11-13.
- Cuenot, N., Dorbath, C., and Dorbath, L., 2008, Analysis of the Microseismicity Induced by Fluid Injections at the Egs Site of Soultz-Sous-Forêts (Alsace, France): Implications for the Characterization of the Geothermal Reservoir Properties. *Pure and Applied Geophysics* **165**, 797-828.
- DiPippo, R., 2012, Chapter 22 - Enhanced Geothermal Systems – Projects and Plants. *Geothermal Power Plants (Third Edition)*, Butterworth-Heinemann, 443-81.
- Evans, K.F., Genter, A., and Sausse, J., 2005, Permeability Creation and Damage Due to Massive Fluid Injections into Granite at 3.5 Km at Soultz: 1. Borehole Observations. *Journal of Geophysical Research: Solid Earth* **110**.
- Hasting, M., Albaric, J., Oye, V., Reid, P., Messeiller, M., Llanos, E., Malin, P., Shalev, E., Hogg, M., Alvarez, M., Miller, A., Walter, C., Boese, C., and Voss, N., 2011, Real Time Induced Seismicity Monitoring During Wellbore Stimulation at Paralana South Australia.
- Heise, W., Bibby, H.M., Caldwell, T.G., Bannister, S.C., Ogawa, Y., Takakura, S., and Uchida, T., 2007, Melt Distribution beneath a Young Continental Rift: The Taupo Volcanic Zone, New Zealand. *Geophysical Research Letters* **34**, L14313.
- Hogarth, R., Holl, H., and McMahon, A., Flow Testing Results from the Habanero Egs Project. *6th Australian Geothermal Energy Conference*, 21-28.
- Holl, H. and Barton, C., Habanero Field-Structure and State of Stress. *Proceedings the World Geothermal Congress*, 19-25.
- Key, K. and Oval, J., 2011, A Parallel Goal-Oriented Adaptive Finite Element Method for 2.5-D Electromagnetic Modelling. *Geophysical Journal International* **186**, 137-54.
- Llanos, E.M., Zarrouk, S.J., and Hogarth, R.A., 2015, Numerical Model of the Habanero Geothermal Reservoir, Australia. *Geothermics* **53**, 308-19.

- MacFarlane, J., Thiel, S., Pek, J., Peacock, J., and Heinson, G., 2014, Characterisation of Induced Fracture Networks within an Enhanced Geothermal System Using Anisotropic Electromagnetic Modelling. *Journal of Volcanology and Geothermal Research* **288**, 1-7.
- McMahon, A. and Baisch, S., 2013, Case Study of the Seismicity Associated with the Stimulation of the Enhanced Geothermal System at Habanero, Australia. *Proceedings Australian Geothermal Conference*, 29-36.
- McMahon, A. and Baisch, S., 2015, Seismicity Associated with the Stimulation of the Enhanced Geothermal System at Habanero, Australia. *Proceedings World Geothermal Congress*, 1-9.
- Meixner, A.J., Kirkby, A.L., and Horspool, N., 2014, Using Constrained Gravity Inversions to Identify High-Heat-Producing Granites beneath Thick Sedimentary Cover in the Cooper Basin Region of Central Australia. *Geothermics* **51**, 483-95.
- Meixner, A.J., Kirkby, A.L., and Lescinsky, D.T., 2012, The Cooper Basin3d Map Version 2: Thermal Modelling and Temperature Uncertainty. Geoscience Australia, Record2012/60.
- Meixner, T.J., Gunn, P.J., Boucher, R.K., Yeates, T.N., Richardson, L.M., and Frears, R.A., 2000, The Nature of the Basement to the Cooper Basin Region, South Australia. *Exploration Geophysics* **31**, 24-32.
- Muñoz, G., 2014, Exploring for Geothermal Resources with Electromagnetic Methods. *Surveys in Geophysics* **35**, 101-22.
- Peacock, J.R., Thiel, S., Heinson, G.S., and Reid, P., 2013, Time-Lapse Magnetotelluric Monitoring of an Enhanced Geothermal System. *Geophysics* **78**, B121-B30.
- Peacock, J.R., Thiel, S., Reid, P., and Heinson, G., 2012, Magnetotelluric Monitoring of a Fluid Injection: Example from an Enhanced Geothermal System. *Geophys. Res. Lett.* **39**, L18403.
- Reynolds, S.D., Mildren, S.D., Hillis, R.R., and Meyer, J.J., 2006, Constraining Stress Magnitudes Using Petroleum Exploration Data in the Cooper–Eromanga Basins, Australia. *Tectonophysics* **415**, 123-40.
- Reynolds, S.D., Mildren, S.D., Hillis, R.R., Meyer, J.J., and Flottmann, T., 2005, Maximum Horizontal Stress Orientations in the Cooper Basin, Australia: Implications for Plate-Scale Tectonics and Local Stress Sources. *Geophysical Journal International* **160**, 332-44.
- Rodi, W. and Mackie, R.L., 2001, Nonlinear Conjugate Gradients Algorithm for 2-D Magnetotelluric Inversion. *Geophysics* **66**, 174-87.
- Spichak, V. and Manzella, A., 2009, Electromagnetic Sounding of Geothermal Zones. *Journal of Applied Geophysics* **68**, 459-78.
- Wohlenberg, J. and Keppler, H., 1987, Monitoring and Interpretation of Seismic Observations in Hot Dry Rock Geothermal Energy Systems. *Geothermics* **16**, 441-45.
- Yanagisawa, N., Matsunaga, I., Ngothai, Y., and Wyborn, D., Geochemistry Change During Circulation Test of Egs System. *Proceedings of the Thirty-Sixth Workshop on Geothermal Reservoir Engineering*.
- Zhang, S., Paterson, M.S., and Cox, S.F., 1994, Porosity and Permeability Evolution During Hot Isostatic Pressing of Calcite Aggregates. *Journal of Geophysical Research: Solid Earth* **99**, 15741-60.
- Ziagos, J., Phillips, B.R., Boyd, L., Jelacic, A., Stillman, G., and Hass, E., A Technology Roadmap for Strategic Development of Enhanced Geothermal Systems. *Proceedings of the 38th Workshop on Geothermal Reservoir Engineering, Stanford, CA*, 11-13.